ISSN 0567-7351
CN 31-1320/O6
CODEN HHHPA4
http://sioc-journal.cn

化学学报

ACTA CHIMICA SINICA

2017 第75卷 第6期 Vol. 75 No. 6

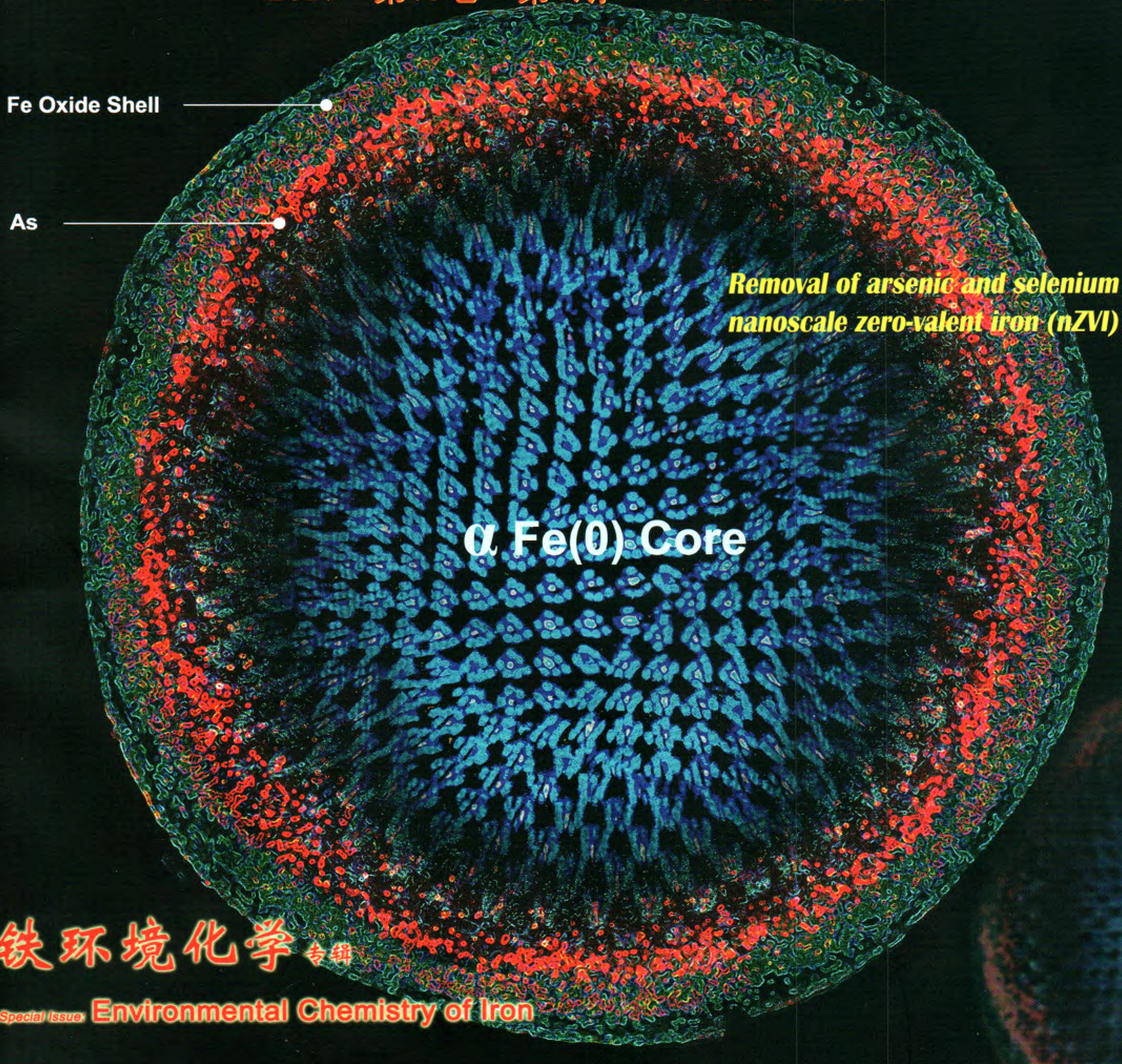

铁环境化学专辑

Special Issue: Environmental Chemistry of Iron

ISSN 0567-7351
9 770567 735172 06>

中国化学会
中国科学院上海有机化学研究所 主办

化 学 学 报

Acta Chimica Sinica

(Huaxue Xuebao)

第 75 卷　第 6 期　2017 年 6 月 15 日

目　次

社论

研究评论

研究展望

综述

研究论文

---

* 通信联系人.

ACTA CHIMICA SINICA

Vol. 75, No. 6 June 15, 2017

Contents

On the cover: A nanostructure-based mechanism of encapsulation is presented on the enrichment, separation and immobilization of selenium and arsenic with zero-valent iron nanoparticles. Experimental results demonstrates the rapid separation, large capacity, stability and unique properties of iron nanoparticles for treatment and remediation of toxic heavy metals such as selenium, chromium, arsenic, uranium *etc*. [Ling, Lan *et al.* on page 594-601.]

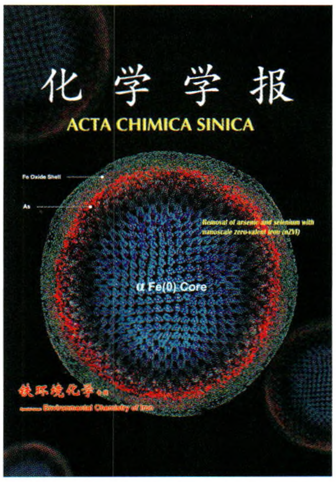

On the back cover: Fe(II)-catalyzed phase transformation of iron (hydr)oxides is the important chemical reaction of iron cycle in anaerobic environments, such as paddy soils. Through electron transfer and Fe atom exchange reaction mechanisms, ferrihydrite was transformed to lepidocrocite, goethite, and magnetite when catalyzed by Fe(II). With coexisted Pb(II), the phase transformation of ferrihydrite was inhibited and the transformed products were changed due to the competitive adsorption of Pb(II) with Fe(II) on the ferrihydrite surface, while Pb(II) was stabilized in the structures of transformed iron (hydr)oxides. [Li, Fangbai *et al.* on pages 621-628.]

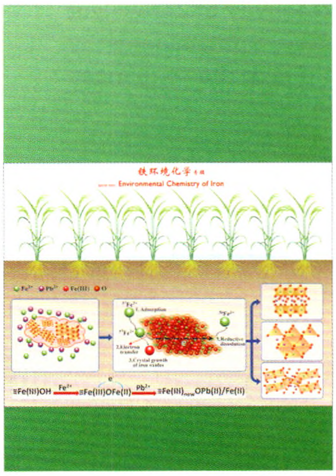

Editorial

Account

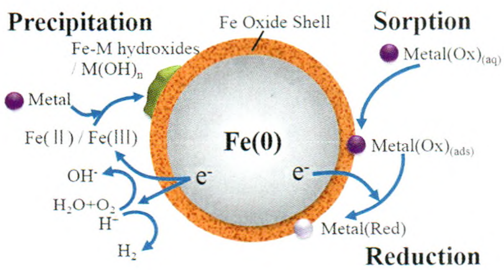

Nanoscale zero-valent iron (nZVI) is a perfect example of core-shell structured and multifunctional nanomaterials for environmental applications, and has rich surface chemistry. The unique core-shell structure and the surface chemistry endow nZVI with unique and multifaceted functions for heavy metal removal including sorption, reduction and precipitation.

Molecular Oxygen Activation with Nano Zero-valent Iron for Aerobic Degradation of Organic Contaminants and the Performance Enhancement

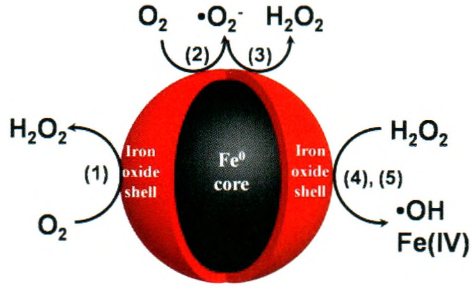

$O_2 + Fe^0 + 2H^+ \rightarrow Fe^{2+} + H_2O_2$ (1)

$O_2 + Fe^{2+} \rightarrow Fe^{3+} + \bullet O_2^-$ (2)

$\bullet O_2^- + Fe^{2+} + 2H^+ \rightarrow Fe^{3+} + H_2O_2$ (3)

$H_2O_2 + Fe^{2+} \rightarrow Fe^{3+} + \bullet OH + OH^-$ (4)

$H_2O_2 + Fe^{2+} + 2H^+ \rightarrow Fe(IV) + 2H_2O_{\ (pH \geq 5)}$ (5)

Mu, Yi; Jia, Falong; Ai, Zhihui*; Zhang, Lizhi*

Acta Chim. Sinica **2017**, *75*(6), 538-543

Generally, the core-shell structured nano zero-valent iron induced molecular oxygen activation and reactive oxygen species generation simultaneously involved a two-electron molecular oxygen activation pathway through the outward electron transfer from the iron core to the iron oxide shell surface and a single-electron molecular oxygen activation by the surface bound Fe(II) on the iron oxide shell.

Improving the Reactivity of Zerovalent Iron toward Various Contaminants by Weak Magnetic Field: Performances and Mechanisms

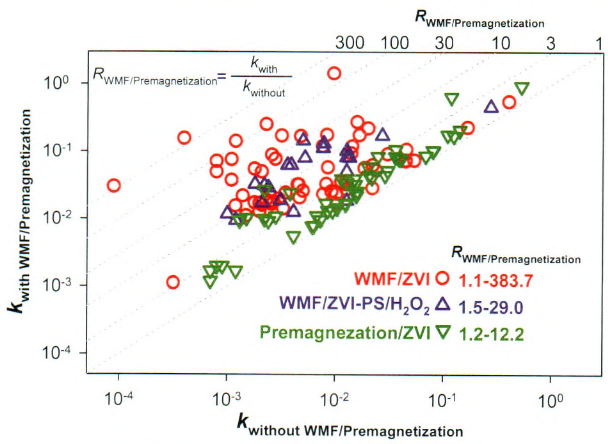

Li, Jinxiang; Qin, Hejie; Zhang, Xueying; Guan, Xiaohong*

Acta Chim. Sinica **2017**, *75*(6), 544-551

The reactivity of ZVI in various reaction systems toward numerous contaminants were increased by 1.1～383.7 folds due to WMF superimposition or premagnetization.

Perspective

Biomineralization: a Pivotal Process in Developing a Novel Passive Treatment System for Acid Mine Drainage

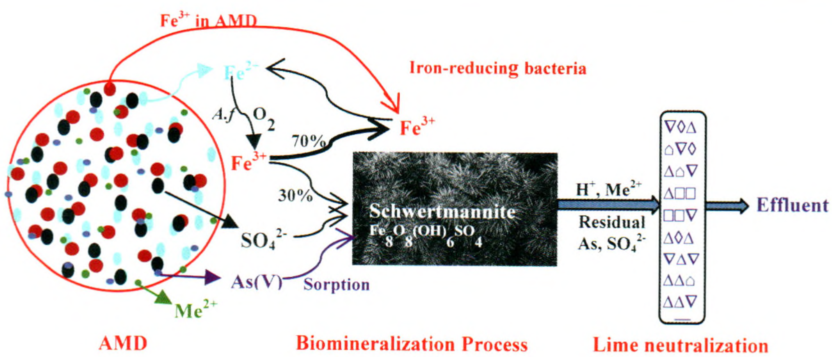

Zhou, Lixiang*

Acta Chim. Sinica **2017**, *75*(6), 552-559

This perspective shows how AMD is purified through biomineralization of soluble iron and sulfate facilitated by iron-oxidizing and iron-reducing bacterial and subsequent lime neutralization.

Review

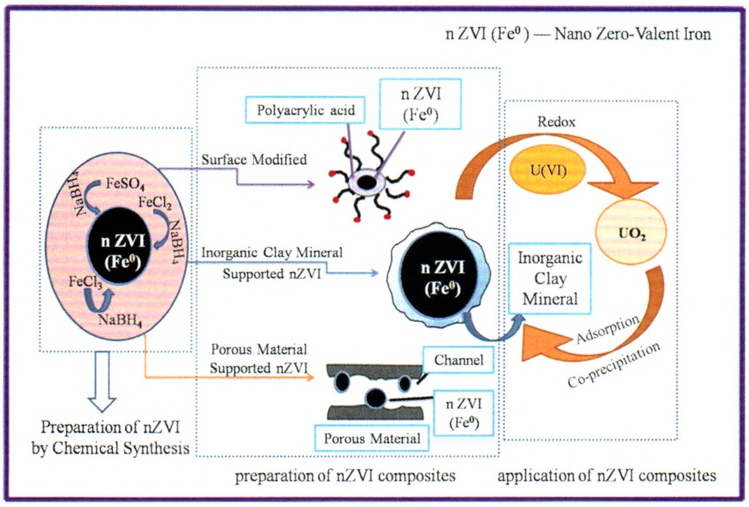
n ZVI (Fe⁰) — Nano Zero-Valent Iron
Polyacrylic acid
n ZVI (Fe⁰)
Surface Modified
Redox
U(VI)
UO₂
FeSO₄
FeCl₂
NaBH₄
FeCl₃
n ZVI (Fe⁰)
Inorganic Clay Mineral Supported nZVI
Inorganic Clay Mineral
Adsorption
Co-precipitation
Porous Material Supported nZVI
Channel
Porous Material
Preparation of nZVI by Chemical Synthesis
preparation of nZVI composites
application of nZVI composites

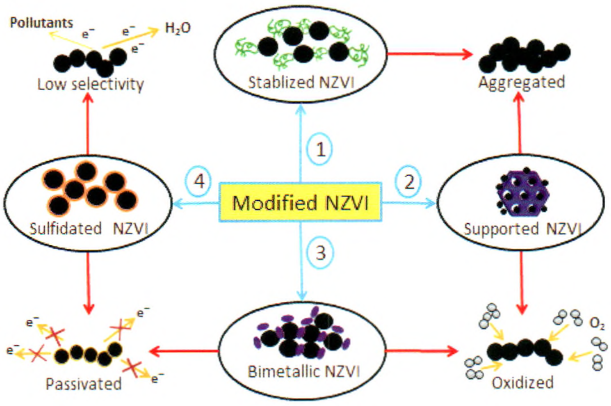
Pollutants
H₂O
Low selectivity
Stablized NZVI
Aggregated
Sulfidated NZVI
Modified NZVI
Supported NZVI
Passivated
Bimetallic NZVI
Oxidized
O₂

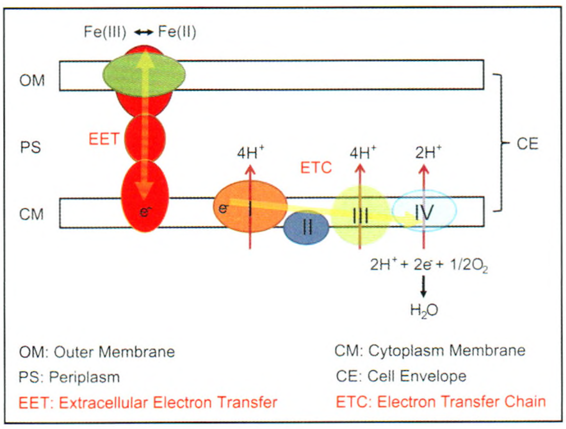
Fe(III) ↔ Fe(II)
OM
PS
CM
CE
EET
ETC
4H⁺
4H⁺
2H⁺
I
II
III
IV
2H⁺ + 2e⁻ + 1/2O₂
H₂O
OM: Outer Membrane
PS: Periplasm
EET: Extracellular Electron Transfer
CM: Cytoplasm Membrane
CE: Cell Envelope
ETC: Electron Transfer Chain

Article

Removal of Arsenic and Selenium with Nanoscale Zero-Valent Iron (nZVI)

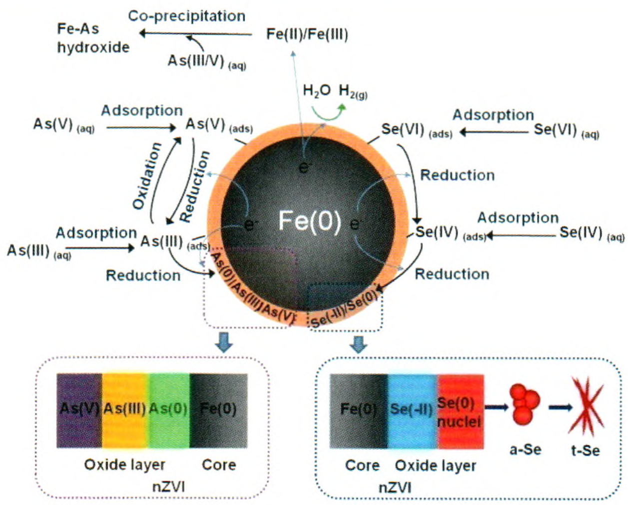

Xia, Xuefen; Hua, Yilong; Huang, Xiaoyue; Ling, Lan*; Zhang, Weixian*

Acta Chim. Sinica **2017**, *75*(6), 594-601

Nanoscale zero-valent iron (nZVI) has a remarkable capability to remove As and Se from aqueous solutions. The removal performances of nZVI for As(III), As(V), Se(IV) and Se(VI) were different due to the different reaction mechanisms. Arsenic (As(III/V)) can be removed by the synergistic effects of adsorption, reduction and co-precipitation. Meanwhile, aqueous Se(IV/VI) was first immobilized by adsorption, and then reduced to Se(0)/Se(-II). Especially, pure Se(0) nanostructures could be generated under ambient temperature and pressure.

Copper Ions Promoted Aerobic Atrazine Degradation by $Fe@Fe_2O_3$ Nanowires

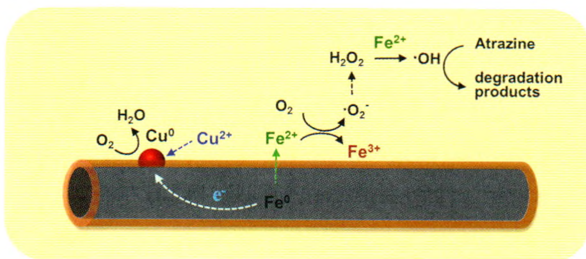

Jia, Falong; Liu, Juan; Zhang, Lizhi*

Acta Chim. Sinica **2017**, *75*(6), 602-607

The addition of Cu^{2+} could enhance the rate of aerobic atrazine degradation with $Fe@Fe_2O_3$ nanowires because of the efficient release of Fe^{2+} ions and the molecular oxygen activation.

Influences and Mechanisms of As(V) Concentration and Environmental Factors on Hydrosulfate Green Rust Transformation

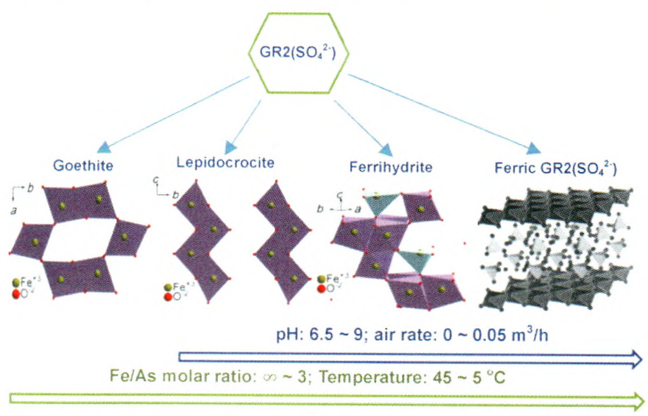

Wang, Xiaoming; Peng, Jing; Xu, Huanhuan; Tan, Wenfeng; Liu, Fan; Huang, Qiaoyun; Feng, Xionghan*

Acta Chim. Sinica **2017**, *75*(6), 608-616

With increasing As(V) concentration, the transformation products of $GR2(SO_4^{2-})$ change from mixed phases of goethite and lepidocrocite to pure lepidocrocite to mixed phases of lepidocrocite, ferrihydrite, and ferric $GR2(SO_4^{2-})$. When Fe/As molar ratio is 24, lepidocrocite is the main product at the conditions of pH 6.5～9, temperature of 5～45 ℃, and air rate of 0～0.05 m^3/h. High pH and air rate, and low temperature favor the formation of ferrihydrite and ferric $GR2(SO_4^{2-})$.

Fe(III)-induced Sequestration of Citric Acid on Kaolinite Surface Probed by STXM-NEXAFS Spectroscopy

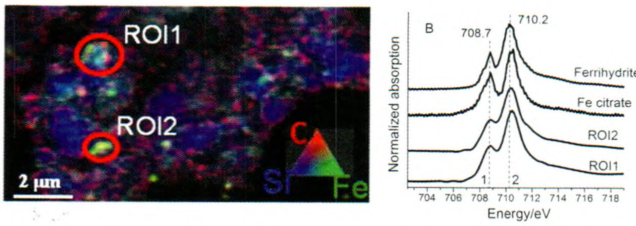

Liu, Jin; Yang, Jianjun*; Zeng, Xibai; Wang, Jian*; Donald Sparks

Acta Chim. Sinica **2017**, *75*(6), 617-620

Submicron-scale co-distribution of C, Fe and Si at the selected hot spots 1 and 2 (ROI1, ROI2), together with the blue shift of peak 2 at 710.2 eV in the Fe $L_{3,2}$-edge NEXAFS spectra of ROI1 compared to that of ROI2, occurred in the investigated sorption sample from kaolinite-Fe(III)-citric acid (CA) system at a Fe/CA molar ratio of 2.0 with initial pH = 3.0.

Adsorption and Stabilization of Lead during Fe(II)-catalyzed Phase Transformation of Ferrihydrite

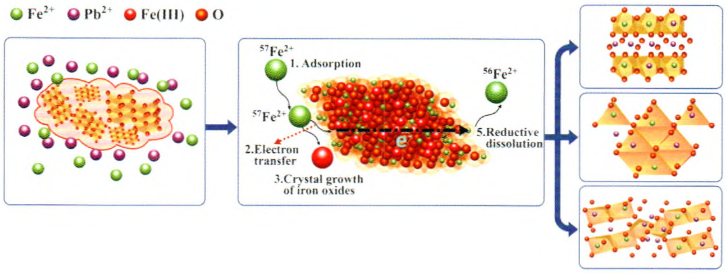

Liu, Chengshuai; Li, Fangbai*; Chen, Manjia; Liao, Changzhong; Tong, Hui; Hua, Jian

Acta Chim. Sinica **2017**, *75*(6), 621-628

With the coexisting Pb(II), Fe(II)-catalyzed phase transformation of ferrihydrite was inhibited due to the competitive adsorption of Pb(II) with Fe(II) on the surface of ferrihydrite. Through electron transfer and Fe atom exchange reaction mechanisms, ferrihydrite was transformed to lepidocrocite, goethite, and magnetite catalyzed by Fe(II), in which Pb(II) was stabilized in the structures of these transformed iron (hydr)oxides.

Identification Influence Mechanism of Humic Acid in the Degradation of Decabromodiphenyl Ether by the BC@Ni/Fe Nanoparticles

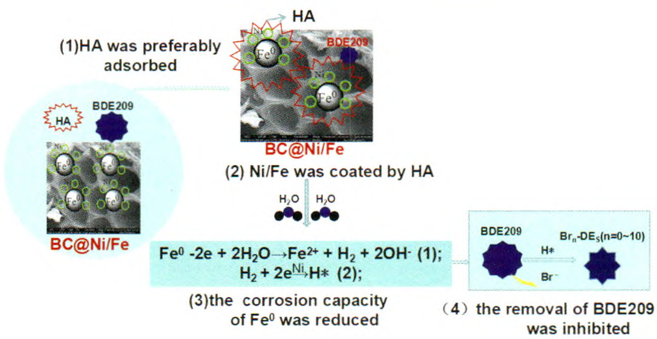

Yi, Yunqiang; Wu, Juan; Fang, Zhanqiang*

Acta Chim. Sinica **2017**, *75*(6), 629-636

The adsorbed HA coated on the surface of BC@Ni/Fe occupied the active sites, which hindered the nanoparticles to contact with H_2O, reduced the corrosion of Fe^0, thus inhibited the removal of BDE209.

The Acid-Base Buffer Capacity of Red Soil Variable Charge Minerals and Its Surface Complexation Model

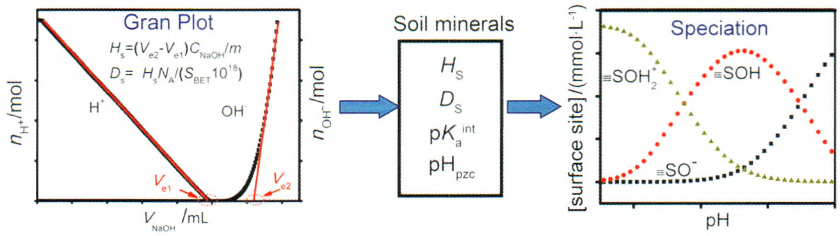

Cheng, Pengfei; Wang, Ying; Cheng, Kuan; Li, Fangbai; Qin, Haoli; Liu, Tongxu*

Acta Chim. Sinica **2017**, *75*(6), 637-644

The acid-base property parameters of variable charge minerals were obtained by Gran plots with the 1-site/2-pK surface complexation model. These parameters, including their surface active sites concentration (H_s) and density (D_s), their acid-base equilibrium constants (pK_a^{int}) and the charge zero pH_{pzc}, can reflect the acid-base buffer capacity of the soil minerals and further be used to predict the speciation distribution of red soil minerals under different pH.

ISSN 0567-7351
CN 31-1320/O6
CODEN HHHPA4
http://sioc-journal.cn

化 学 学 报

ACTA CHIMICA SINICA

2017 第75卷 第6期 Vol. 75 No. 6

铁环境化学专辑

Special Issue: Environmental Chemistry of Iron

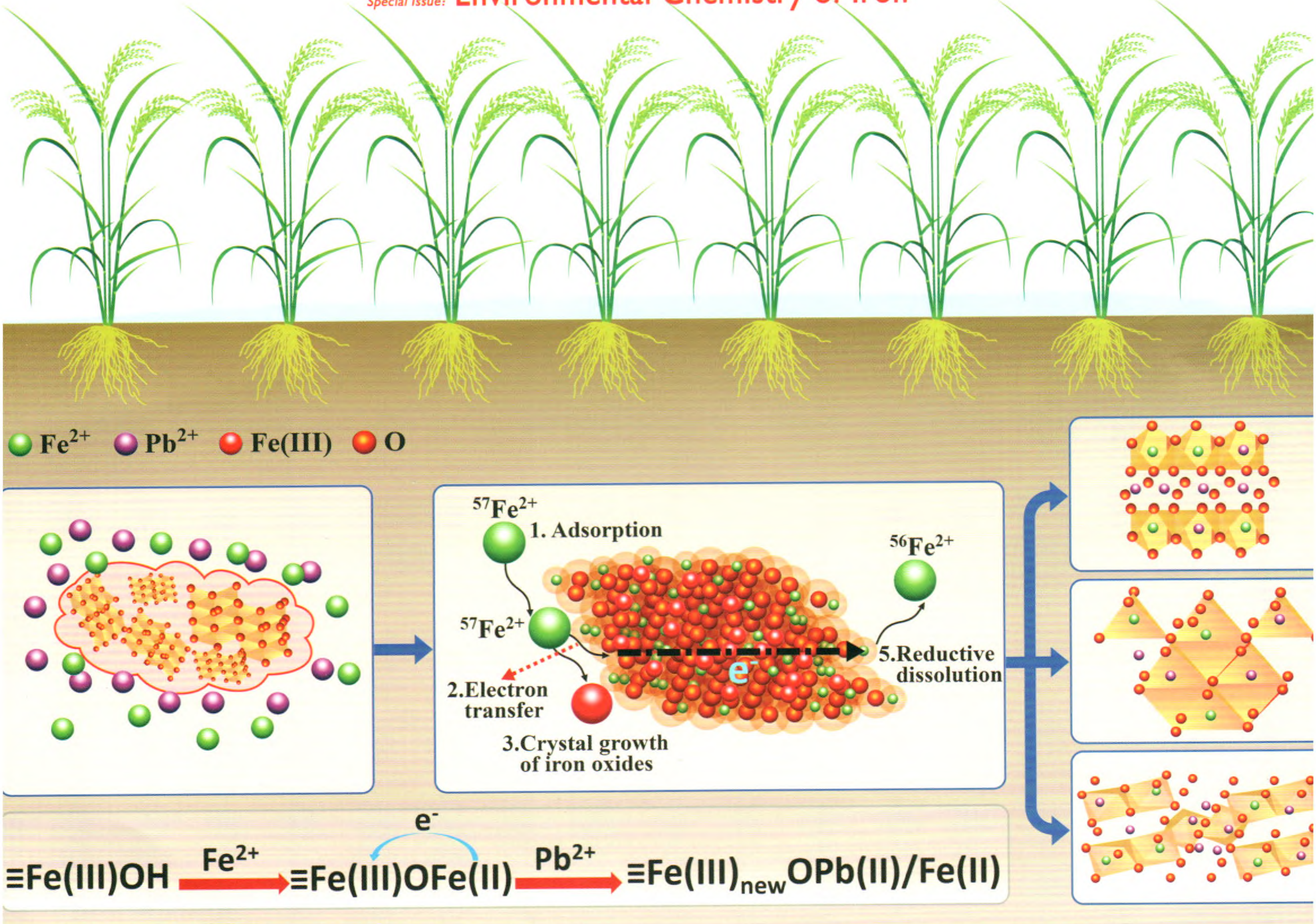

ISSN 0567-7351
06>

中国化学会
中国科学院上海有机化学研究所
主办